NANO MICRO small

On-Electrode Synthesis of Shape-Controlled Hierarchical Flower-Like Gold Nanostructures for Efficient Interfacial DNA Assembly and Sensitive Electrochemical Sensing of MicroRNA

Shao Su, Yan Wu, Dan Zhu, Jie Chao, Xingfen Liu, Ying Wan, Yan Su, Xiaolei Zuo, Chunhai Fan, and Lianhui Wang**

The performance for biomolecular detection is closely associated with the interfacial structure of a biosensor, which profoundly affects both thermodynamics and kinetics of the assembly, binding and signal transduction of biomolecules. Herein, it is reported on a one-step and template-free on-electrode synthesis method for making shape-controlled gold nanostructures on indium tin oxide substrates, which provide an electrochemical sensing platform for ultrasensitive detection of nucleic acids. Thus-prepared hierarchical flower-like gold nanostructures (HFGNs) possess large surface area that can readily accommodate the assembly of DNA probes for subsequent hybridization detection. It is found that the sensitivity for electrochemical DNA sensing is critically dependent on the morphology of HFGNs. By using this new strategy, a highly sensitive electrochemical biosensor is developed for label-free detection of microRNA-21 (miRNA-21), a biomarker for lung cancers. Importantly, it is demonstrated that this biosensor can be employed to measure the miRNA-21 expression level from human lung cancer cell (A549) lysates and worked well in 100% serum, suggesting its potential for applications in clinical diagnosis and a wide range of bioanalysis.

Prof. S. Su, Y. Wu, D. Zhu, Prof. J. Chao, Prof. X. Liu, Prof. C. Fan, Prof. L. Wang
Key Laboratory for Organic Electronics & Information Displays (KLOEID)
Institute of Advanced Materials (IAM)
National Synergistic Innovation Center for Advanced Materials (SICAM)
Nanjing University of Posts &Telecommunications
9 Wenyuan Road, Nanjing 210023, China
E-mail: fchh@sinap.ac.cn; iamlhwang@njupt.edu.cn
Prof. Y. Wan, Prof. Y. Su
School of Mechanical Engineering
Nanjing University of Science and Technology
Nanjing 210094, China
Prof. X. Zuo, Prof. C. Fan
Division of Physical Biology
Shanghai Institute of Applied Physics
Chinese Academy of Sciences
Shanghai 201800, China

DOI: 10.1002/smll.201601066

1. Introduction

Since the great development of electrochemical sensor due to its unique advantages, such as high sensitive, specific, convenient and low-cost, it has been considered as a powerful tool for the environmental monitoring,[1] food safety,[2] genetic analysis,[3] and clinical diagnostics.[4,5] To enhance its sensitivity, selectivity, and stability, nanomaterials have been introduced into constructing electrochemical sensor due to their unique merits (e.g., large surface-to-volume ratio, excellent electronic/mechanical/catalytic properties, etc.), such as graphene,[6] silicon nanowires,[7] carbon nanotubes,[8] molybdenum disulfide (MoS_2),[9] and noble metallic nanomaterials.[10,11] For example, Li's group and Wang's group had reviewed the development of graphene-based electrochemical sensors for diverse bioassays, from simple molecules to complex biotargets.[12,13] Zhang et al. combined gold nanoparticles-based nanoamplifier with a "sandwich" detection strategy for ultrasensitive detection of DNA. The detection

limit of this electrochemical sensor was estimated to be 10 fM target DNA.[14] Su et al. developed a label-free electrochemical immunosensor for carcino-embryonic antigen (CEA) detection based on gold nanoparticles (AuNPs)-decorated thionine–MoS_2 nanocomposite, which could detect as low as 0.52 pg mL^{-1} CEA with excellent selectivity.[15]

Among these nanomaterials, gold nanomaterials have been extensively applied in electrochemical sensors because of their high electrical/thermal conductivities, easy functionalization, and good biocompatibility. More interestingly, the properties of gold nanomaterials were greatly depended on their size and morphology. Therefore, shape-controlled gold nanostructures (such as particles, rods, wires, cubes, stars, flowers, and dendrites) have been synthesized by different methods.[16] Hierarchical flower-like gold nanostructures (HFGNs) have recently been attracted great research interests due to their high surface areas and special shapes, making them as promising candidates for fabrication of chemical and biological sensors. The introduction of HFGNs into the electrochemical sensors could efficiently increase the specific biosensing surface and amounts of probe molecules, which could obviously enhance the performances of those sensors. Zhang et al. employed electrodeposition method to fabricate hierarchical waxberry-like gold nanostructures on glass carbon electrode. The as-prepared gold nanostructures possessed high active surface area, which showed high electrocatalytic responses to the reduction of oxygen and the oxidation of glucose.[17] Kelley's group electrodeposited hierarchical gold nanostructures on chips to fabricate multiplex arrays, which could measure protein biomarkers CA-125 in human serum and whole blood with high sensitivity.[4] Shi et al. one-step prepared hierarchically aloe-like gold micro-/nanostructures as an electrochemical platform for ultrasensitive DNA recognition. Using AuNPs as an amplifier, the DNA biosensor displayed a significantly enhanced detection limit of 12 aM with good selectivity, stability, and reusability.[18] Such exciting works proved that hierarchical gold nanostructure might be a potential and valuable electrochemical sensing platform. However, the size and morphology of hierarchical gold nanostructures in modulating biodetection sensitivity have been less addressed and needs further exploration in detail.

Herein, shape-controlled gold nanostructures were successfully synthesized on ITO surface by electrodeposition method without any templates assisted. The sizes and morphologies of gold nanostructures were tuned by altering electrodeposition conditions (**Figure 1**a). As we know, different sizes and morphologies of gold nanostructures possess different surface areas, resulting in different electrochemical performances. Therefore, four typical gold nanostructures were chosen as detection platforms to study the influence of sizes and morphologies of gold nanostructures on biodetection sensitivity, such as spherical gold nanostructures, leaves-like gold dendrites, smooth HFGNs, and rough HFGNs. On the basis of experimental results, a smooth HFGNs-based label-free electrochemical biosensor was designed for miRNA-21 detection (Figure 1b). $Ru(NH_3)_6^{3+}$ was employed as electrochemical signal molecule, which bound to anionic phosphate of DNA/miRNA strands in a stoichiometric approach DNA/miRNA sequences. Therefore, a higher electrochemical signal was obtained in the presence of target miRNA. The as-prepared biosensor had a wide line response ranging from 1 fM to 10 pM and a low detection limit of 1 fM for miRNA-21. Moreover, the HFGNs-based biosensor was also used to monitor miRNA-21 from human lung cancer cells (A549) and cervical cancer cells (HeLa) and exhibited high sensitivity and selectivity toward target miRNA-21 in serum samples. The proposed HFGNs were highly recommended as an efficient biosensing platform for biomolecule immobilizations and bioassays.

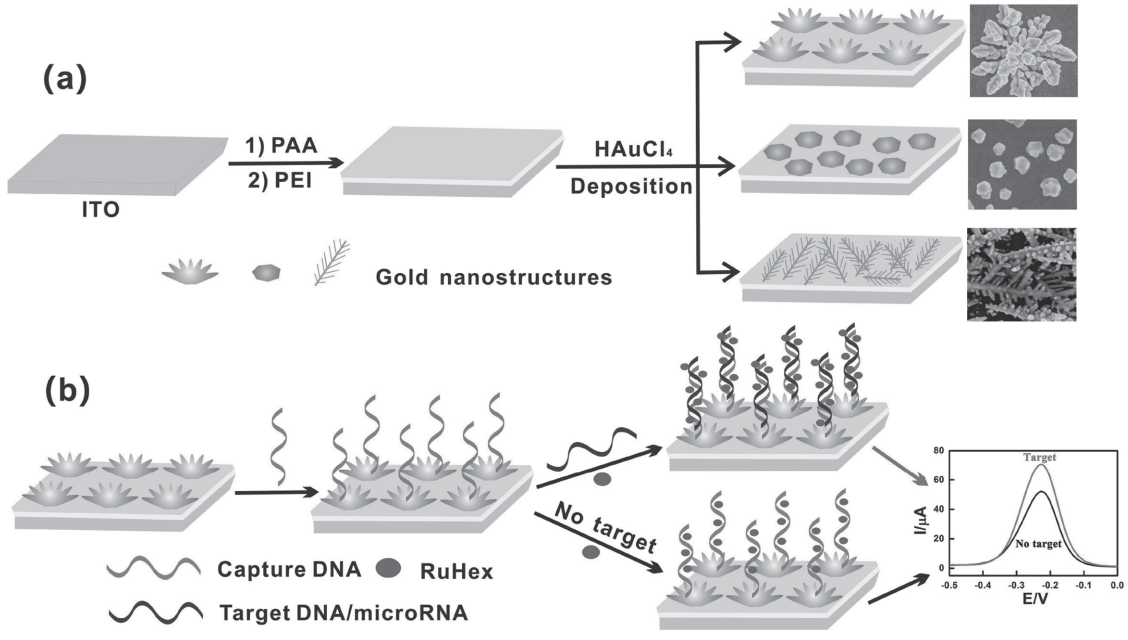

Figure 1. a) Schematic of synthesizing gold nanostructures by electrodeposited method on ITO. b) Illustration of gold nanostructure-based electrochemical biosensor for nucleic acid detection.

small 2016,
DOI: 10.1002/smll.201601066

2. Results and Discussion

2.1. Synthesis and C haracterization of Shape-Controlled HFGNs

The polyelectrolyte multilayer plays a crucial role in forming HFGNs.[19] As shown in Figure S1 (Supporting Information), spherical gold nanostructures were located sparsely on the bare ITO electrode. As expected, well-defined HFGNs were grown on polyelectrolyte-decorated ITO electrode. Moreover, these 3D HFGNs were larger and more stable than spherical gold nanostructures. The reason may be attributed to polyelectrolyte multilayer provided fewer pinholes for nucleation and growth of the nanoparticles and offered a microenvironment to assist HFGNs growth. Therefore, we chose the polyelectrolyte-decorated ITO electrode in our experiments.

To understand the growth influence factors of gold nanostructures, different electrodeposition parameters were investigated, including deposition potential, $HAuCl_4$ concentration, deposition time, and composition of electrolyte. As we know, the morphology of gold nanostructures strongly depended on the deposition potential by using electrodeposition method.[20] Therefore, the potential influence on gold nanostructures was first explored ranging from 0.3 V to –0.3 V. As shown in **Figure 2**, different sizes and morphologies of gold nanostructures were obtained by using different potentials in 0.50×10^{-3} M $HAuCl_4$ for 30 min. Large quantities of well-defined gold nanostructures were dispersed on the ITO surface with a diameter of ≈1.77 μm at 0.3 V (Figure 2A). A higher-magnification image (inset in Figure 2A) further revealed that these nanostructures were flower-like morphologies, which built with many nanoflakes as building blocks in a staggered way. As the potential shifted from 0.3 V to –0.3 V (Figure 2A–H), the gold nanostructures ranged from well-defined hierarchical flower-like (Figure 2A) to simple flower-like (Figure 2B,C), spherical (Figure 2D), irregular nanostructures (Figure 2E) and dendritic-type morphologies (Figure 2F–H). Moreover, the crystal density also increased with the potential negative shift. It should be noted that dendritic-type with many arms and branches gold nanostructures were obtained when the potential was –0.3 V (Figure 2H). Unfortunately, these dendritic-type gold nanostructures easily fell off the ITO surface during the washing process. To synthesize shape-controlled and well-defined gold nanostructures, 0.3 V was chosen in the following experiment.

The $HAuCl_4$ concentration and supporting electrolyte also greatly influenced the sizes and morphologies of HFGNs. **Figure 3** showed the SEM images of gold nanostructures formed on ITO at 0.3 V for 30 min in different concentration of $HAuCl_4$ solution ranging from 0.12×10^{-3} M to 1.52×10^{-3} M. The diameter of gold nanostructures was increased from 779 nm to 3.75 μm with the concentration of $HAuCl_4$ increased from 0.12×10^{-3} M to 0.64×10^{-3} M (Figure 3A–E). Moreover, the morphology of gold nanostructures was gradually prone to hierarchical flower-like with $HAuCl_4$ concentration increased (inset in Figure 3A–E). It was noted that high-quality and well-defined HFGNs were obtained when the precursor concentration was 0.50×10^{-3} M (Figure 3D). If $HAuCl_4$ concentration was over 0.50×10^{-3} M, the arms of gold nanostructures increased and the size of gold nanostructures continually grew bigger (Figure 3E–I). More interestingly, the HFGNs became more complicated if the $HAuCl_4$ concentration increasing from 0.64×10^{-3} M to 1.62×10^{-3} M. From the purpose of economical and shape-controlled, 0.50×10^{-3} M $HAuCl_4$ was used to obtained well-defined HFGNs in this work. On the basis of above results, the influence of electrolyte was also studied. Unexpectedly, well-defined gold nanostructure was also obtained when the electrolyte containing NaCl, which was similar to that without NaCl (Figure S2, Supporting Information). Many small particles decorated on gold nanostructures, resulting in the prepared HFGNs were much rougher than these obtained without NaCl.[21]

Figure 4 showed the morphological evolution of the HFGNs at 0.3 V for varying deposition time in 0.50×10^{-3} M $HAuCl_4$ solution. With deposition time increasing, it was a tendency that gold nanostructures grew bigger and more complicated. Below 60 s, small and few HFGNs were dispersed on the ITO surface, which were built by several smaller

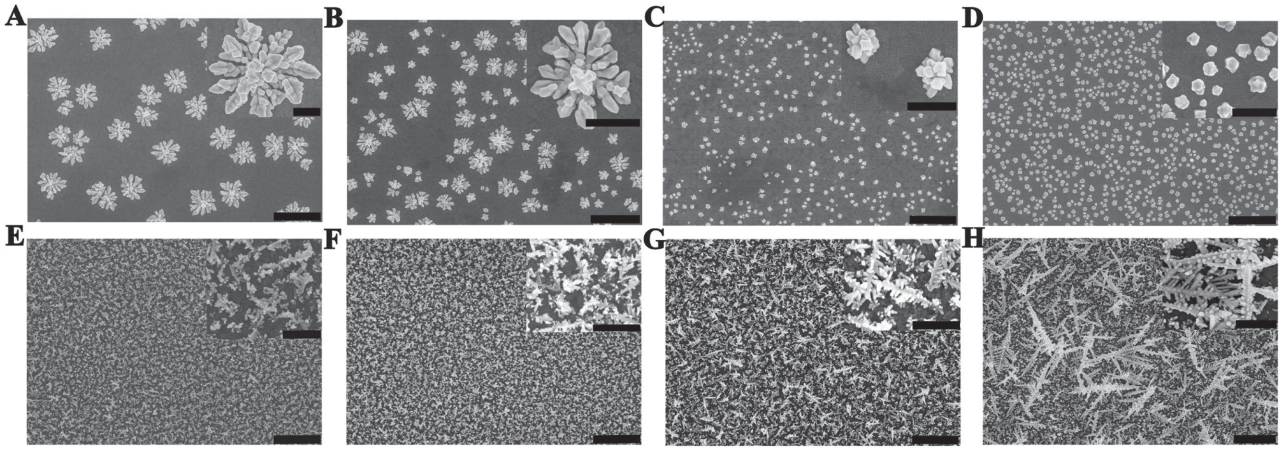

Figure 2. SEM images of gold nanostructures formed on a polyelectrolyte multilayer modified ITO at different deposition potential: A) 0.3 V, B) 0.2 V, C) 0.15 V, D) 0.1 V, E) –0.1 V, F) –0.15 V, G) –0.2 V and H) –0.3 V in 0.5×10^{-3} M $HAuCl_4$ solution for 30 min. Scale bars correspond to 2 μm. Inset: corresponding higher-magnification SEM images of gold nanostructures. Scale bars correspond to 500 nm.

DOI: 10.1002/smll.201601066

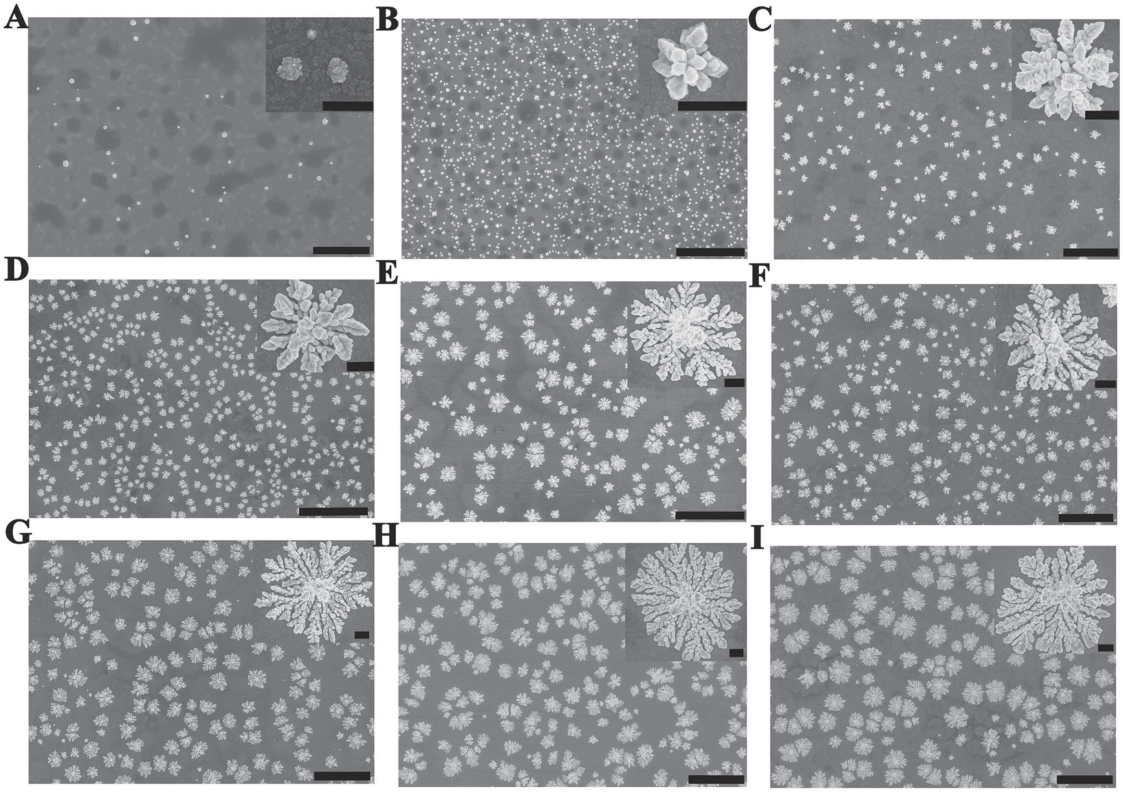

Figure 3. SEM images of gold nanostructures formed on a polyelectrolyte multilayer modified ITO at 0.3 V for 30 min in A) 0.12×10^{-3} M, B) 0.26×10^{-3} M, C) 0.38×10^{-3} M, D) 0.50×10^{-3} M, E) 0.64×10^{-3} M, F) 0.76×10^{-3} M, G) 1.10×10^{-3} M, H) 1.22×10^{-3} M, and I) 1.52×10^{-3} M $HAuCl_4$ solution. Scale bars correspond to 10 μm. Inset: corresponding higher-magnification SEM images of gold nanostructures. Scale bars correspond to 500 nm.

particles (Figure S3, Supporting Information). HFGNs grew bigger and possessed higher density if the deposition time prolonged ranging from 60 s to 3600 s (Figure 4A–I). It should be noticed that the growth of gold onto the nuclei and the formation of new nuclei were simultaneously occurred in the 0–300 s (Figure 4A–D). If the deposition time over 300 s, the growth of gold onto the nuclei dominated the morphology of gold nanostructures, leading to larger and larger HFGNs formation (Figure 4E–I). Uniform and well-defined HFGNs were obtained when the deposition time was 1800 s (Figure 4H). If the deposition time over 1800 s, gold nanostructures continuously grew bigger and more branches were observed. Unfortunately, some gold nanostructures became aggregated and irregularly, resulting in the number of gold nanostructures decreased (Figure 4I). Therefore, 1800 s was chosen as the optimal deposition time.

The composition and crystal structure of typical HFGNs were investigated by EDX and XRD, respectively. The EDX spectrum confirmed that pure Au nanostructures were formed by electrodeposition method (Figure S4, Supporting Information). The XRD patterns of HFGN exhibited sharp diffraction peaks corresponding to the (111), (200), (220) diffractions, indicating that this nanostructure was face-centered cubic (fcc) Au crystals (JCPDS No. 04-0784, Figure S5, Supporting Information). The UV–vis absorption spectroscopy was also used to monitor HFGMs by altering $HAuCl_4$ concentration. Figure S6 (Supporting Information) showed the absorption spectra of gold nanostructures deposited on the ITO surface had an obvious red shift from 567 to 673 nm with the concentration of $HAuCl_4$ increasing from 0.12×10^{-3} M to 0.64×10^{-3} M at 0.3 V for 1800 s (from curve e to curve a). The color of the ITO surface changed from purple to red with the concentration of $HAuCl_4$ increasing (inset in Figure S6, Supporting Information). The size of the deposited gold nanostructures became larger and the distance between the adjacent gold nanostructures became narrower with increasing the concentration of $HAuCl_4$, which produced the enormous local electromagnetic enhancement and resulted in the absorption peak red-shift.[22,23] This result was agreement with the SEM images of gold nanostructures, which shown in Figure 3A–E. All the results suggested the obtained nanostructures were gold nanostructures. To understand the growth mechanism of HFGNs, a chronoaperometic method was used to study the nucleation and crystal growth mechanism (Figure S7, Supporting Information).[18] According to the SEM images and *i–t* curves, the growth mechanism of HFGNs was proposed in this work. It could be explained by a two-staged growth model: initial nanoblocks and subsequent accumulated growth. At first stage, many Au nuclei were uniformly grown on the ITO surface via instantaneous reduction of Au^{3+} ion to metallic Au. Then, the subsequent growth of gold crystals would preferentially occur onto the preformed gold nuclei rather than on a bare ITO surface through a surface reaction, which is possibly due to the relatively high activation energy for the surface reaction.[24–26]

DOI: 10.1002/smll.201601066

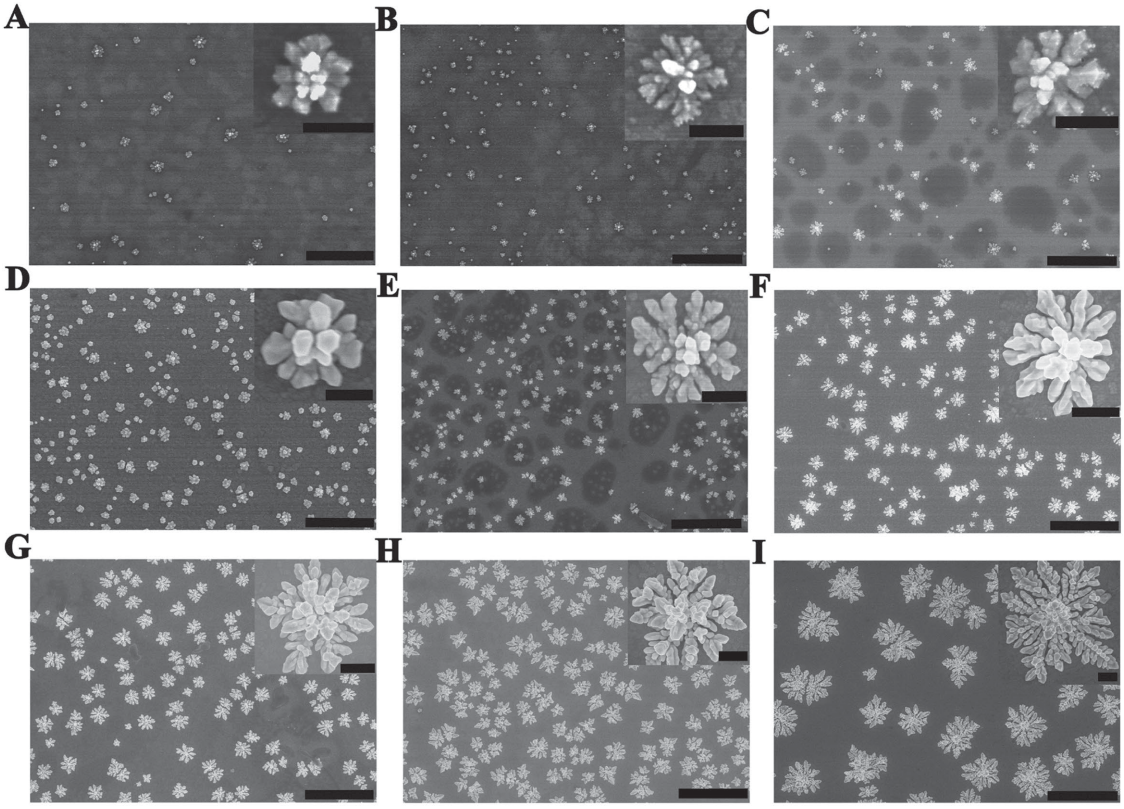

Figure 4. SEM images of gold nanostructures electrodeposited on ITO surface at 0.3 V for A) 60 s, B) 120 s, C) 180 s, D) 300 s, E) 600 s, F) 900 s, G) 1200 s, H) 1800 s, and I) 3600 s in 0.50×10^{-3} M $HAuCl_4$ solution. Scale bars correspond to 5 μm. Inset: corresponding higher-magnification SEM images of gold nanostructures. Scale bars correspond to 500 nm.

2.2. Electrochemical Performance of HFGNs

To select better gold nanostructure as a sensing platform, how nanostructure influenced the sensitivity of electrochemical sensor was first explored. Four typical gold nanostructures, spherical gold nanostructures (Figure 2D), leaves-like gold dendrites (Figure 2H), smooth HFGNs (Figure 2A) and rough HFGNs (Figure S2B, Supporting Information) were selected to construct label-free electrochemical biosensor for DNA detection. In our system, $Ru(NH_3)_6^{3+}$ was employed as electrochemical probe molecule, which bound to anionic phosphate of DNA strands in a stoichiometric approach DNA sequences.[14] Therefore, the electrochemical signals of these biosensors were largely depended on the total amount of DNA probes assembled on these gold nanostructures. As shown in **Figure 5**, the linear ranges and detection limits of these gold nanostructures were dramatically influenced by the fineness of the nanostructure. The detailed SWV curves of four electrochemical sensors were displayed in Figure S8 (Supporting Information). The linear ranges and detection limits of both smooth and rough HFGNs/ITO were 1 fM–100 pM and 1 fM, respectively. The detection limit of leaves-like gold dendrites microelectrode (100 aM) was lower than HFGNs microelectrode, but the linear range was narrower than that of it (100 aM–100 fM). For spherical nanostructures, it only detected as low as 10 fM target DNA, which was higher than HFGNs/ITO. These results were similar to Kelley's group previous work, but the detection limit was higher than this report.[27] Bin et al. have reported that nanostructuring of sensor could determine the efficiency of biomolecular capture.[28] They found that the rough nanostructures possess high capture efficiency than that of smooth nanostructures. As we know, probe density and capture efficiency greatly influence the detection limit of DNA biosensor. In general, moderate probe density and high capture

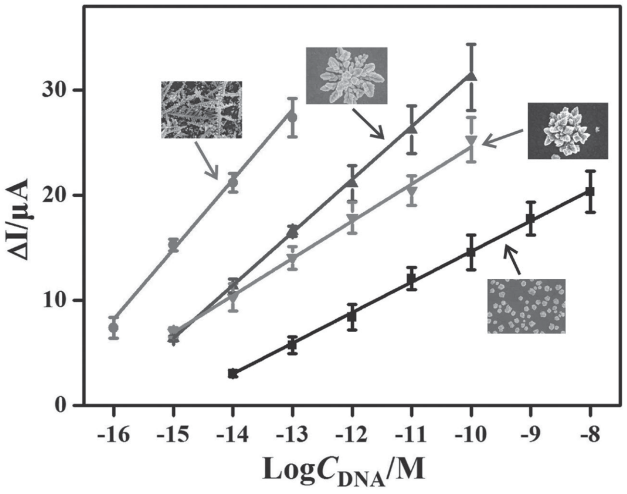

Figure 5. Comparison of the detection performances of four typical gold nanostructures with different morphologies.

DOI: 10.1002/smll.201601066

efficiency result in low detection limit. Therefore, a biosensor with larger surface area and rough nanostructuring could accommodate more DNA probe and possess higher capture efficiency, leading to lower detection limit. Combined with SEM images, leaves-like gold dendrites nanostructures had larger surface area and rougher nanostructuring than other three nanostructures, which exhibited the lowest detection limit. Unfortunately, such gold dendrites nanostructures could fell off ITO surface if the ITO electrode immersed in solution for long time, resulting in the electrochemical signal disappeared. Compared with other gold nanostructures, smooth HFGNs is more uniform and shape-controlled. Moreover, the electrochemical signal enhancement ($\Delta I = I_{target} - I_{no\ target}$) of smooth HFGNs-based biosensor was larger than that of rough HFGN-based biosensor. Therefore, we chose smooth HFGNs as electrochemical platform for label-free microRNA detection in this work.

2.3. HFGNs-Based Biosensors for MicroRNA Detection in Buffer and Real Sample

Aspired by above results, well-defined and smooth HFGNs were chosen to construct electrochemical biosensor for miRNA-21 detection. Figure S9 (Supporting Information) showed the peak current of HFGNs-based biosensor was increased with the concentration of target miRNA-21 increasing. Under the optimal condition, the ΔI was linear correlation to the logarithm of the miRNA-21 concentrations ranged from 1 fM to 10 pM with a detection limit of 1 fM (**Figure 6**A). It should be noted that the ΔI of RNA detection was lower than that of DNA detection under the same concentration. Because some miRNA-21 might be degraded during the process of hybridization, resulting in the amount of miRNA-21 hybridized with probe DNA was lower than theoretical value. The specificity of the HFGNs-based electrochemical biosensor was also investigated. The ΔI for single-base mismatched, two-base mismatched and random miRNA sequence was about 37%, 20%, and 4% of that for perfectly matched miRNA-21 at the same concentration, respectively, indicating that this biosensors possessed excellent selectivity (Figure 6B). On the basis of above results, we also used this biosensor to analyze miRNA-21 expression level from different cancerous cell lines, such as human lung cancer cells (A549) and cervical cancer cells (HeLa). As shown in Figure 6C, the current responses of this biosensor incubated with the lysate from A549 cells (10^6 cells) was much larger than that with HeLa cells (10^6 cells), indicating that miRNA-21 was overexpressed in A549 cells, which was good agreement with the previous reports.[29,30] More importantly, the current responses of this biosensor increased with the number of A549 cells increasing (Figure 6D). The HFGNs-based biosensor could detect as low as 100 A549 cells, which was comparable to or lower than other literatures.[31,32]

Finally, the HFGNs-based biosensor challenged to analyze miRNA-21 in 100% serum sample. Figure S10 (Supporting Information) showed the electrochemical signal of HFGNs-based sensor increased with miRNA-21 concentration

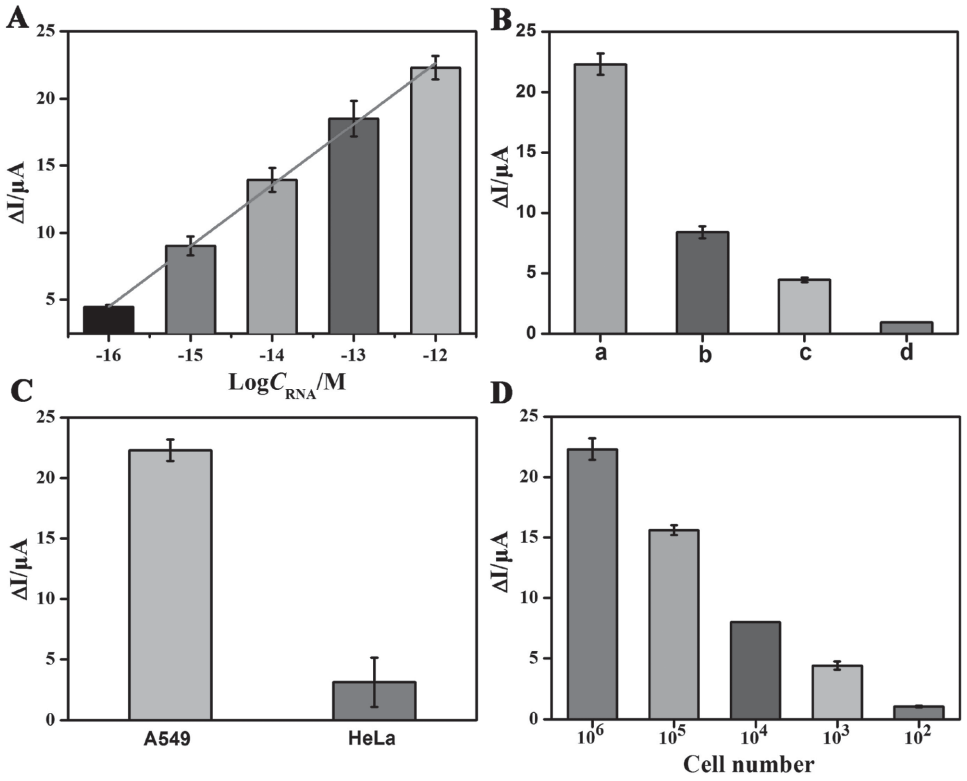

Figure 6. A) Calibration plots of ΔI versus logarithm of the miRNA-21 concentrations from 1 fM to 10 pM. B) The ΔI of (a) target miRNA, (b) single-base mismatched, (c) two-base mismatched, and (d) random miRNA sequences. C) Electrochemical signal of HFGNs-based biosensor for detection of miRNA-21 extracted from A549 cell and HeLa cell. D) Detection of miRNA-21 with HFGNs-based sensor in lysates ranging from 10^2 to 10^6 A549 cells.

small 2016,
DOI: 10.1002/smll.201601066

increasing from 1 fM to 10 pM in 100% serum, which was similar to the miRNA detection in buffer. However, the ΔI of 1 fM miRNA-21 in 100% serum (3.1 μA) was smaller than that in buffer (4.4 μA). This biosensor could work well even in 100% serum, suggesting the HFGNs-based biosensor have a great potential in early diagnosis of diseases in real samples.

2.4. Reproducibility, Regeneration, and Stability of the Fabricated Biosensor

The repeatability, regeneration, and stability of the fabricated biosensor were extremely important for the practical applications. Five parallel HFGNs-based electrochemical biosensors were used to detect 1.0×10^{-13} M target miRNA. The relative standard deviation (RSD) of electrochemical signals was 8.5% ($n = 5$), indicating high reproducibility of HFGNs-based electrochemical biosensor. The regeneration ability was also evaluated according to previous works.[33] Briefly, the fabricated electrode was dipped in hot water (80 °C) for 15 min and then rapidly cooled in the ice bath for 10 min. It was found that the fabricated biosensor could be regenerated 11 times with about 29% loss of the original signal, which was comparable to or better than some reported works (Figure S11, Supporting Information).[33,34] At the same time, the stability of the fabricated biosensor was also investigated. The DNA probe modified HFGNs/ITO was first stored in the refrigerator at 4 °C, and then examined after the hybridization with complementary miRNA strands at interval over 3 d. Experimental data demonstrated that the DNA biosensor retained about 84% of its initial response even after 15 d.

3. Conclusion

In this work, shape-controlled and well-defined gold nanostructures have been synthesized by using a simple and one-step electrodeposition method. SEM was used to monitor the size and morphology regulation by changing electrodeposition conditions. Four typical gold nanostructures have been selected to study the nanostructure influence of electrochemical performance, such as sensitivity and stability. On the basis of experimental results, HFGNs were selected as electrochemical sensing platform for highly sensitive and selective miRNA-21 detection in buffer and real sample due to its excellent electrochemical properties and easy preparation. Due to the excellent performance, such gold nanostructures (HFGNs) maybe a potential detection platform combined with electrochemistry, surface plasma resonance or surface-enhanced Raman scattering technique for biological and chemical molecules detection.

4. Experimental Section

Chemicals and Materials: Gold(III) chloride trihydrate ($HAuCl_4 \cdot 3H_2O$, ≥47.8%) was obtained from Alfa Aesar, 6-mercapto-1-hexanol (MCH, 97%), poly(acrylic acid) (PAA), poly(ethyleneimine) (PEI), and hexaammineruthenium(III) chloride ($Ru(NH_3)_6^{3+}$) were purchased from Sigma Aldrich. C_2H_5OH, (hydroxymethy)aminomethane, $(CH_3)_2CO$, NaCl, NaH_2PO_4, and Na_2HPO_4 were brought from Sinopharm Chemical Reagent Co., Ltd. The commercial glass slides coated with a layer of 50 nm indium tin oxide (ITO) with resistance of 8 Ω sq^{-1} were used as conductive substrates. Water (18.2 MΩ cm) was obtained from an ultrafilter system (Milli-Q, Millipore, MA). DNA and RNA oligonucleotides were synthesized and purified by TAKARA Biotechnology (Table S1, Dalian, China).

Methods and Apparatus: Chronoamperometry (CA), cyclic voltammetry (CV) and square wave voltammetry (SWV) were operated on an Autolab PGSTAT302 (Metrohm China Ltd, Switzerland). The electrochemical experiments were tested by a conventional three-electrode system, in which a HFGNs/ITO, a Pt wire, and a saturated calomel electrode (SCE) were employed as a working electrode, a counter electrode, and a reference electrode, respectively. Nitrogen bubbling was needed to restrain oxygenation in electrolyte solutions for at least 30 min and the electrochemical measurements were carried out under a nitrogen atmosphere. The morphologies of the as-prepared HFGNs were observed by scanning electron microscopy (SEM, Hitachi S4800). The properties of HFGNs were determined by UV–VIS–NIR spectra (UV-3600). DNA immobilization buffer: 10×10^{-3} M Tris-HCl containing 0.1 M NaCl (pH 7.4). Hybridization buffer: 10×10^{-3} M phosphate buffered saline with 0.25 M NaCl (PBS, pH 7.4). RNA Hybridization buffer: 25×10^{-3} M PBS (pH 7.4) with 0.25 M NaCl.

Fabrication of Gold Nanostructures via the Electrochemical Deposition: In this experiment, ITO (geometric area = 1 cm^2) was ultrasonic cleaned sequentially in acetone, ethanol, and distilled water for 1 h, respectively. Then, a polyelectrolyte multilayer (six bilayers of PEI/PAA) was used as preformed matrix to adjust the morphology of HFGNs in electrochemical deposition, which was fabricated by layer-by-layer self-assembly technique. Different electrodeposition parameters have been investigated during the process of HFGNs synthesis, such as deposition potentials (–0.3–0.3 V), deposition time (0–3600 s), $HAuCl_4$ concentrations ($0.12–1.52 \times 10^{-3}$ M) and composition of electrolyte (with or without Cl^-).

Immobilization and Hybridization of DNA and RNA Sequences: At first, the HFGNs/ITO electrode was incubated in the immobilization solution containing 200×10^{-9} M of thiolated cDNA for 16 h at room temperature. Then, the unbound cDNA was washed away by using PBS and distilled water. After that, the cDNA-modified HFGNs/ITO electrode was further treated with 10×10^{-3} M MCH solution for 2 h to passivate the unreacted active spots. The modified HFGMs/ITO electrode was then immersed in the hybridization buffer containing a series of concentration of target DNA/miRNA sequence to form double-stranded DNA (dsDNA)-modified electrode for 1 h. Finally, the proposed HFGNs/ITO electrode was washed successively with PBS, distilled water, and then dried with nitrogen gas.

Electrochemical Measurements: Electrochemical signals were measured in 10×10^{-3} M PB solution (pH 7.4) containing 100×10^{-9} M $Ru(NH_3)_6^{3+}$ and 25×10^{-3} M NaCl. Electrochemical signals were collected in the absence and presence of target DNA/miRNA by SWV using a potential step of 5 mV, pulse amplitude of 50 mV, pulse width of 50 ms, and a pulse period of 100 ms in this experiment. At least three independent trials were used to obtain each data in this article.

DOI: 10.1002/smll.201601066

Supporting Information

Supporting Information is available from the Wiley Online Library or from the author.

Acknowledgements

This work was financially supported by the National Basic Research Program of China (2012CB933301), the National Natural Science Foundation of China (21305070, 21475064), the Natural Science Foundation of Jiangsu Province (BK20130861), the Sci-tech Support Plan of Jiangsu Province (BE2014719), the Program for Changjiang Scholars and Innovative Research Team in University (IRT_15R37), and the Priority Academic Program Development of Jiangsu Higher Education Institutions (PAPD, YX03001).

[1] S. Su, W. Wu, J. Gao, J. Lu, C. Fan, *J. Mater. Chem.* **2012**, *22*, 18101.
[2] B. Pérez-López, A. Merkoçi, *Trends Food Sci. Technol.* **2011**, *22*, 625.
[3] H. Yang, A. Hui, G. Pampalakis, L. Soleymani, F. Liu, E. Sargent, S. Kelley, *Angew. Chem. Int. Ed.* **2009**, *48*, 8461.
[4] J. Das, S. O. Kelley, *Anal. Chem.* **2011**, *83*, 1167.
[5] R. Cui, C. Liu, J. Shen, D. Gao, J. Zhu, H. Chen, *Adv. Funct. Mater.* **2008**, *18*, 2197.
[6] X. Zuo, S. He, D. Li, C. Peng, Q. Huang, S. Song, C. Fan, *Langmuir* **2010**, *26*, 1936.
[7] S. Su, Y. He, M. Zhang, K. Yang, S. Song, X. Zhang, C. Fan, S.-T. Lee, *Appl. Phys. Lett.* **2008**, *93*, 023113.
[8] H. Chen, X. Zuo, S. Su, Z. Tang, A. Wu, S. Song, D. Zhang, C. Fan, *Analyst* **2008**, *133*, 1182.
[9] S. Su, H. Sun, F. Xu, L. Yuwen, L. Wang, *Electroanalysis* **2013**, *25*, 2523.
[10] J. Yang, E. Sargent, S. Kelley, J. Y. Ying, *Nat. Mater.* **2009**, *8*, 683.
[11] Y. Wan, Y. Zhou, M. Poudineh, T. Safaei, R. Monjamadi, E. Sargent, S. Kelley, *Angew. Chem. Int. Ed.* **2014**, *53*, 13145.
[12] Y. Fang, E. Wang, *Chem. Commun.* **2013**, *49*, 9526.
[13] D. Chen, H. Feng, J. Li, *Chem. Rev.* **2012**, *112*, 6027.
[14] J. Zhang, S. Song, L. Zhang, L. Wang, H. Wu, D. Pan, C. Fan, *J. Am. Chem. Soc.* **2006**, *128*, 8575.
[15] S. Su, M. Zou, H. Zhao, C. Yuan, Y. Xu, C. Zhang, L. Wang, C. Fan, L. Wang, *Nanoscale* **2015**, *7*, 19129.
[16] M. C. Daniel, D. Astruc, *Chem. Rev.* **2004**, *104*, 293.
[17] H. Zhang, J.-J. Xu, H.-Y. Chen, *J. Phys. Chem. C* **2008**, *112*, 13886.
[18] L. Shi, Z. Chu, Y. Liu, W. Jin, X. Chen, *Biosens. Bioelectron.* **2013**, *49*, 184.
[19] X. Zhang, F. Shi, X. Yu, H. Liu, Y. Fu, Z. Wang, L. Jiang, X. Li, *J. Am. Chem. Soc.* **2004**, *126*, 3064.
[20] L. Huang, E.-S. Lee, K.-B. Kim, *Colloids Surf., A* **2005**, *262*, 125.
[21] P. Zhang, L. Chen, T. Xu, H. Liu, X. Liu, J. Meng, G. Yang, L. Jiang, S. Wang, *Adv. Mater.* **2013**, *25*, 3566.
[22] K. M. Mayer, J. H. Hafner, *Chem. Rev.* **2011**, *111*, 3828.
[23] J. Wang, X. Cao, L. Li, T. Li, R. Wang, *J. Phys. Chem. C* **2013**, *117*, 15817.
[24] B. Nikoobakht, M. A. El-Sayed, *Chem. Mater.* **2003**, *15*, 1957.
[25] B.-K. Pong, H. I. Elim, J.-X. C hong, W. Ji, B. L. Trout, J.-Y. Lee, *J. Phys. Chem. C* **2007**, *111*, 6281.
[26] T. H. Lin, C. W. Lin, H. H. Liu, J. T. Sheu, W. H. Hung, *Chem. Commun.* **2011**, *47*, 2044.
[27] L. Soleymani, Z. Fang, E. H. Sargent, S. O. Kelley, *Nat. Nanotechnol.* **2009**, *4*, 844.
[28] X. M. Bin, E. H. Sargent, S. O. Kelley, *Anal. Chem.* **2010**, *82*, 5928.
[29] R. Grogory, K. Yan, G. Amuthan, T. Chendrimada, B. Doratotaj, N. Cooch, R. Shiekhatar, *Nature* **2004**, *432*, 235.
[30] H. Dong, J. Lei, H. Ju, F. Zhi, H. Wang, W. Guo, Z. Zhu, F. Yan, *Angew. Chem. Int. Ed.* **2012**, *51*, 4607.
[31] Y. Liao, R. Huang, Z. Ma, Y. Wu, X. Zhou, D. Xing, *Anal. Chem.* **2014**, *86*, 4596.
[32] D. Zhu, L. Zhang, W. Ma, S. Lu, X. Xing, *Biosens. Bioelectron.* **2015**, *65*, 152.
[33] L. Shi, Z. Chu, Y. Liu, W. Jin, X. Chen, *Biosens. Bioelectron.* **2013**, *49*, 184.
[34] L. Wang, X. Chen, X. Wang, X. Han, S. Liu, C. Zhao, *Biosens. Bioelectron.* **2011**, *30*, 151.

Received: March 29, 2016
Published online:

DOI: 10.1002/smll.201601066